Available online at www.sciencedirect.com

ScienceDirect

Procedia Computer Science 239 (2024) 1387–1392

Procedia Computer Science

www.elsevier.com/locate/procedia

CENTERIS – International Conference on ENTERprise Information Systems / ProjMAN – International Conference on Project MANagement / HCist – International Conference on Health and Social Care Information Systems and Technologies 2023

Seasonal spatial-temporal variability in radar penetration depth

Sergey Samsonov*

Canada Centre for Mapping and Earth Observation, Natural Resources Canada, 580 Booth Street, Ottawa, ON, K1A 0E4, Canada

Abstract

A fully automated processing system for measuring long-term ground deformation time series and deformation rates frame-by-frame using the Differential Interferometric Synthetic Aperture Radar (DInSAR) processing technique was developed and tested. Among the several factors that affect DInSAR's precision, such as temporal decorrelation and atmospheric noise, it was observed that seasonal spatial-temporal variability in radar penetration depth is the greatest contributor to the loss of precision of the long-term deformation rate measurement. This spatial-temporal signal is described for a specific region in the northern US; however, it is widely observed in multiple regions. In these regions, a gradual penetration depth increase is observed in fall and winter, and an abrupt penetration depth decrease is observed in spring. The latter effect is likely caused by rapid melting of ice and snow that, at the same time, significantly reduces interferometric coherence. Within a specific geographic region, radar penetration depth spatially varies proportionally to the elevation due to an elevation-dependent temperature gradient, producing artifacts that correlate well with the topography. This signal does not extend to high-elevation regions (above ~2500 m) that do not experience seasonal thawing, which allows for distinguishing it from the topography-dependent atmospheric signals. Without accounting for the spatial-temporal variability in radar penetration depth, deformation time series in these areas can contain either an annual periodic signal with an amplitude of over 0.1 m or, if the abrupt penetration depth decrease produced by melting is not resolved due to lower coherence, an erroneous interannual trend. Spatial-temporal variability in radar penetration depth needs to be better understood and corrected to improve the precision of long-term deformation rate products, particularly in regions susceptible to seasonal freezing and thawing.

Keywords: Differential Interferometric Synthetic Aperture Radar; DInSAR; ground deformation; natural hazards; automated processing; operational processing; Multidimensional Small Baseline Subset; MSBAS; radar penetration depth.

* Corresponding author.
E-mail address: sergey.samsonov@nrcan-rncan.gc.ca.

10.1016/j.procs.2024.06.310

1. Introduction

The processing of more than 200,000 Sentinel-1 images over North America and Eurasia generated long-term deformation rate maps available in a public repository [1]. Many novel natural and artificial deformation signals were identified in these results, several of which were slow-moving deep-seated landslides. In multiple regions, it was observed that the deformation signal was contaminated with a noise correlated with topographic relief or land cover types. The deformation time series showed a systematic seasonal pattern. In regions with topographic relief, the signal amplitude increased proportionally to the elevation from the reference. In regions with different land cover types, the amplitude was largest in natural areas when the reference was chosen in urban areas. The preliminary analysis suggested that the observed signal is due to the seasonal spatial-temporal variability in radar penetration depth.

Here we present an example of a Sentinel-1 deformation rate map that shows the signal due to seasonal spatial-temporal variability in radar penetration depth. A first attempt was made to model this signal using a negative-degree day model. While this model explained the observed signal for a single pixel taken from the deformation rate map well, a more robust approach is required for operational processing.

2. Data and methodology

To compute the linear deformation rate and cumulative deformation time series, 146 Sentinel-1 SAR images from path 100, frame 446, were used. Then, 221 differential interferograms with small temporal and spatial baselines were computed using GAMMA software [2]. The topographic phase was estimated and removed using the 30 m resolution Advanced Spaceborne Thermal Emission and Reflection Radiometer (ASTER) Digital Elevation Model (DEM) [3]. Differential interferograms are filtered using adaptive filtering with a filtering function based on the local fringe spectrum [4] and unwrapped using the minimum cost flow algorithm [5]. We used precise orbital information and did not apply an orbital correction. For the time series analysis with the Multidimensional Small Baseline Subset (MSBAS) software [6], deformation maps were resampled to a similar lat/long grid with the Geospatial Data Abstraction Library (GDAL) *gdalwarp* program. Finally, the time series were extracted for several pixels, including the one presented here, located in the region with a significant apparent deformation signal.

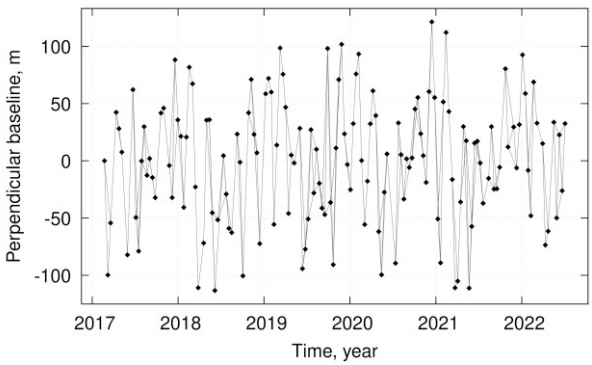

Fig. 1 Temporal and spatial baselines of interferograms used in this study.

3. Results

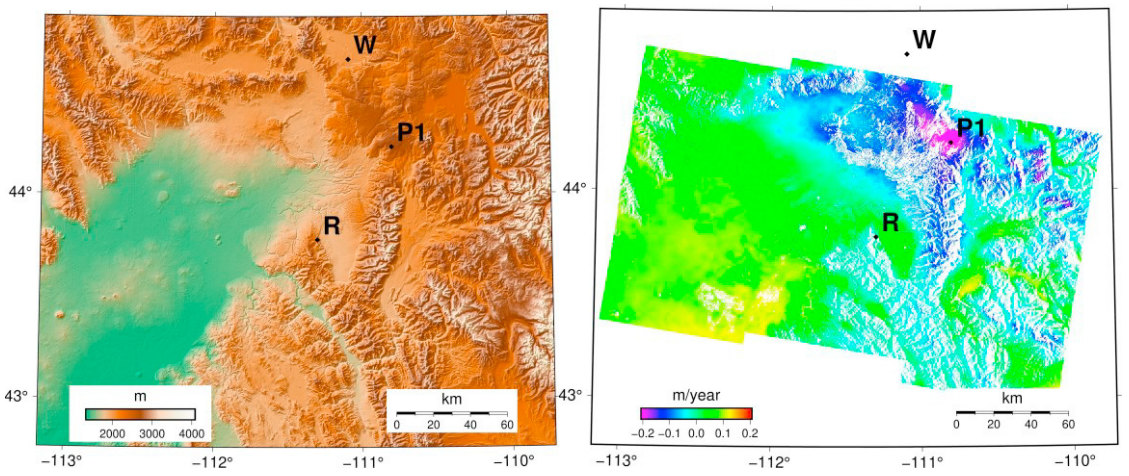

Fig. 2 a) 30 m resolution Advanced Spaceborne Thermal Emission and Reflection Radiometer (ASTER) Digital Elevation Model (DEM) and b) 2017-2022 Sentinel-1 linear deformation rate map. Sites are W is West Yellowstone weather station, R - reference region and P1 - measurement region.

Figure 2a shows surface topography, and Figure 2b shows the 2017-2023 deformation rate map. The observed signal is likely entirely due to seasonal spatial-temporal variability in radar penetration depth. Three sites are marked in Figure 2. The weather station (site W) at which mean daily surface temperatures were recorded, the reference point (site R) that was selected by MSBAS as a reference, and the measurement point (site P1) that correspond to a region of the largest apparent subsidence, at which time series were extracted and which are shown in Figure 3a.

The time series at P1 (Figure 3a) shows overall apparent subsidence, and similar seasonal behaviour is observed each year, with moderate uplift from summer to early fall followed by rapid subsidence from late fall to late spring. The seasonal subsidence amplitude increases with elevation, producing a topography-correlated pattern. In the additional studies not shown here, when ascending and descending data are processed simultaneously to retrieve the east and vertical deformation rates, this signal is only observed in the vertical component, which suggests that ascending and descending deformation maps are similarly affected. Because such a signal is observed in many deformation rate maps worldwide and individual deformation maps with temporal baselines of about one year (from summer-to-summer next year, not used in inversion) do not show any deformation, the presence of active deformation processes is ruled out.

The stratified atmospheric noise is also ruled out as a source of this signal because this signal is only observed at moderate elevations, depending on the region, at elevations approximately less than ~2500 m. It is particularly apparent in deformation rate maps computed over central British Columbia in Canada in frames covering areas with high topographic relief. This observation suggests that the seasonal water freezing-thawing cycle causes this signal because the surface remains frozen all year at higher elevations. The late fall to late spring interferograms retains high coherence suggesting that the dry snow, if present, remains transparent to SAR.

To compare the observed deformation signal with surface temperatures, we applied a negative degree day model shown in red in Figure 3a. This model conceptually is simple. It suggests that the amount of freezing, as a proxy of penetration depth, is proportional to the cumulative negative temperature. The daily surface mean temperature is measured at the weather station W. Because it is located at a lower elevation than P, a temperature offset T_0 is also estimated. The equations are shown in the insert in Figure 3a with T_0 equal to -3.3°C and k equal to 0.00022 m/°C, determined through inverse modelling.

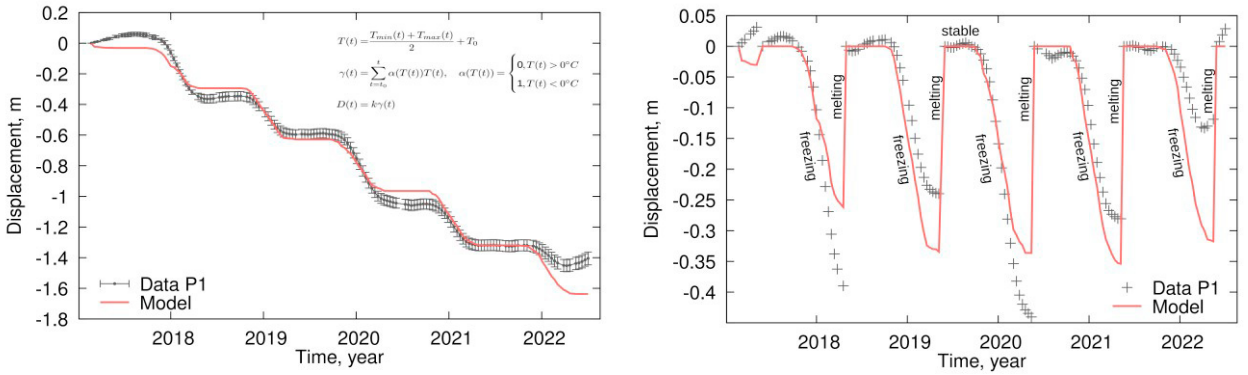

Fig. 3 a) Cumulative (black) and modelled (red) apparent deformation times series. b) Same as in (a), but if phase jump due to rapid surface melt is properly resolved.

It is believed that the phase jump in interferograms computed from SAR images, acquired one before and one after the thawing, is not resolved in the time series in Figure 3a. If it was correctly resolved, it is expected that the actual deformation time series would look like Figure 3b. Here the timing of the discontinuity is estimated from the modelled data as the time when the mean daily temperature becomes positive.

4. Discussion and Conclusions

It was demonstrated that long-term deformation rate measurements can be contaminated with the signal due to the seasonal change in radar penetration depth. During summer to early fall, the penetration depth fluctuates with precipitation. In late fall, surface temperature decreases below zero, causing water to freeze and the penetration depth to increase. This process continues all winter and early spring until a rapid surface melting occurs. If the deformation map that spans the surface melt remained coherent and properly unwrapped, it would have captured a rapid uplift, completing the annual cycle, such as in Figure 3b. This process likely occurs worldwide where the surface temperature fluctuates between positive and negative values; it is almost simultaneous in areas with slight topographic relief, and DInSAR cannot resolve it because it lacks absolute reference. In areas with significant topographic relief, seasonal temperature decrease occurs earlier at higher elevations, which increases radar penetration depth relative to low-elevation areas, producing the apparent subsiding signal at higher elevations (Figure 4). Such an effect is easier to observe with data with extensive spatial coverage and dense temporal coverage, such as data acquired by Sentinel-1.

A conceptual model based on the negative degree day model was proposed to explain this signal. A correction would need to be applied to remove this signal from the deformation products to improve their precision. This correction can be estimated from the proposed negative degree-day model or, from some other data, perhaps even SAR intensity [8].

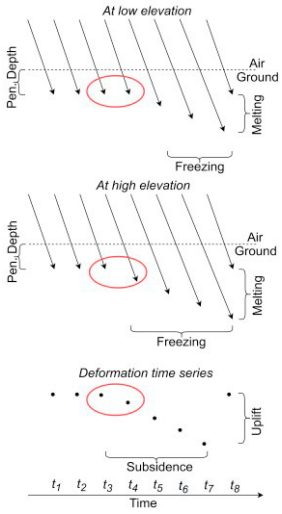

Fig. 4 Schematics of process showing seasonal penetration depth change at two different elevations for one pixel per elevation. At higher elevation, due to colder temperature, ground freezes earlier, producing penetration depth difference that manifests as subsidence.

Signal due to seasonal changes in radar penetration depth was observed in many regions worldwide, specifically Canada, China, Russia, and the USA. No strong correlation between the signal amplitude and the topography was observed because other factors also played an important role (e.g., landcover type - agricultural fields vs. forest). The atmospheric signal resembles a well-formed sine wave with a period equal to one year. It does not affect deformation rates computed over many years [9, 10]. However, the seasonal penetration depth signal discussed here is not fully recoverable; thus, it significantly affects the long-term deformation rates. Additional examples can be found in [11].

Acknowledgements

This work was supported by the Canada Centre for Remote Sensing under the Earth Observation for Cumulative Effects, Phase 2 project. Sentinel-1 data was acquired by the European Space Agency. Images were plotted with GMT and Gnuplot software. GDAL was used for data conversion. Author thanks George Choma of the Canada Centre for Remote Sensing, NRCan, for help with proofreading. NRCan contribution number / Numéro de contribution de RNCan: 20230155.

References

[1] Samsonov, S., Feng, W., 2022. Preliminary retrievals of deformation rates based on 2017-2023 Sentinel-1 data computed with the MSBAS system. Mendeley Data, V.3. doi:10. 17632/t7wvtrk28y.3.
[2] Wegmuller, U., Werner, C., 1997. GAMMA SAR processor and interferometry software, in The 3rd ERS symposium on space at the service of our environment, Florence, Italy, pp. 1687–1692.
[3] Abrams, M., Crippen, R., Fujisada, H., 2020. ASTER Global Digital Elevation Model (GDEM) and ASTER Global Water Body Dataset (ASTWBD). Remote Sensing 12, 1156. doi:10.3390/rs12071156.
[4] Goldstein, R., Werner, C., 1998. Radar interferogram filtering for geophysical applications. Geophys. Res. Lett. 25, 4035–4038. doi:10.1029/1998GL900033.
[5] Costantini, M., 1998. A novel phase unwrapping method based on network programming. IEEE Trans. Geosci. Remote Sens. 36, 813–821. doi:10.1109/36.673674.

[6] Samsonov, S., Dille, A., Dewitte, O., Kervyn, F., d'Oreye, N., 2020. Satellite interferometry for mapping surface deformation time series in one, two and three dimensions: A new method illustrated on a slow-moving landslide. Eng. Geol. 266, 105471. doi:10.1016/j.enggeo.2019.105471.
[7] Nolan, M., Fatland, D., 2003. Penetration depth as a DInSAR observable and proxy for soil moisture. IEEE Trans. Geosci. Remote Sens. 41, 532–537. doi:10.1109/tgrs.2003.809931.
[8] Mironov, V.L., Muzalevsky, K.V., 2013. Spaceborne radar monitoring of soil freezing/thawing processes in the arctic tundra. Russ. Phys. J. 55, 899–902. doi:10.1007/s11182-013-9898-6.
[9] Samsonov, S. V., Trishchenko, A. P., Tiampo, K., González, P. J., Zhang, Y., and Fernández, J. (2014), Removal of systematic seasonal atmospheric signal from interferometric synthetic aperture radar ground deformation time series, Geophys. Res. Lett., 41, 6123–6130, doi:10.1002/2014GL061307.
[10] Samsonov, S. V., Feng, W., and Fialko, Y. (2017), Subsidence at Cerro Prieto Geothermal Field and postseismic slip along the Indiviso fault from 2011 to 2016 RADARSAT-2 DInSAR time series analysis, Geophys. Res. Lett., 44, 2716–2724, doi:10.1002/2017GL072690.
[11] Samsonov, S. V. and Feng, W., 2023. Deformation retrievals for North America and Eurasia from Sentinel-1 DInSAR: big data approach, processing methodology and challenges, Canadian Journal of Remote Sensing, doi: 10.1080/07038992.2023.2247095